

# On the iron oxide neutral cluster distribution in the gas phase. II. Detection through 118 nm single photon ionization

D. N. Shin, Y. Matsuda, and E. R. Bernstein

Citation: *The Journal of Chemical Physics* **120**, 4157 (2004); doi: 10.1063/1.1643733

View online: <http://dx.doi.org/10.1063/1.1643733>

View Table of Contents: <http://aip.scitation.org/toc/jcp/120/9>

Published by the *American Institute of Physics*

---

---

**COMPLETELY**

**REDESIGNED!**



**PHYSICS  
TODAY**

*Physics Today* Buyer's Guide  
Search with a purpose.

# On the iron oxide neutral cluster distribution in the gas phase.

## II. Detection through 118 nm single photon ionization

D. N. Shin, Y. Matsuda, and E. R. Bernstein

*Department of Chemistry, Colorado State University, Fort Collins, Colorado 80523-1872*

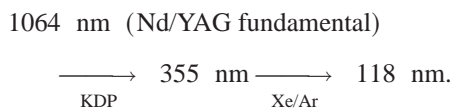
(Received 13 June 2003; accepted 2 December 2003)

Neutral clusters of iron oxide are created by laser ablation of iron metal and subsequent reaction of the gas phase metal atoms, ions, clusters, etc., with an O<sub>2</sub>/He mixture. The Fe<sub>m</sub>O<sub>n</sub> clusters are cooled in a supersonic expansion and detected and identified in a time-of-flight mass spectrometer following laser ionization at 118 nm (10.5 eV), 193 nm (6.4 eV), or 355 nm (3.53 eV) photons. With 118 nm radiation, the neutral clusters do not fragment because single photon absorption is sufficient to ionize all the clusters and the energy/pulse is  $\approx 1 \mu\text{J}$ . Comparison of the mass spectra obtained at 118 nm ionization (single photon) with those obtained at 193 nm and 355 nm ionization (through multiphoton processes), with regard to intensities and linewidths, leads to an understanding of the multiphoton neutral cluster fragmentation pathways. The multiphoton fragmentation mechanism for neutral iron oxide clusters during the ionization process that seems most consistent with all the data is the loss of one or two oxygen atoms. In all instances of ionization by laser photons, the most intense features are of the forms Fe<sub>m</sub>O<sub>m</sub><sup>+</sup>, Fe<sub>m</sub>O<sub>m+1</sub><sup>+</sup>, and Fe<sub>m</sub>O<sub>m+2</sub><sup>+</sup>, and this strongly suggests that, for a given *m*, the most prevalent neutral clusters are of the forms Fe<sub>m</sub>O<sub>m</sub>, Fe<sub>m</sub>O<sub>m+1</sub>, and Fe<sub>m</sub>O<sub>m+2</sub>. As the value of *m* increases, the more oxygen rich neutral clusters appear to increase in stability. © 2004 American Institute of Physics. [DOI: 10.1063/1.1643733]

### I. INTRODUCTION

Given that knowledge of the neutral cluster distribution of metal oxide clusters is an essential component for the elucidation of reactivity and catalytic behavior of such systems, the problem of cluster fragmentation in the process of their detection must be addressed.<sup>1</sup> Since small metal oxide particles (M<sub>x</sub>O<sub>y</sub>, 1 ≤ *x*, *y* ≤ 100) typically have an enormous density of vibronic states and thus, poorly resolved spectra and very rapid relaxation processes, their study and characterization is typically through mass spectroscopy. Ionization of such neutral clusters is most gently done by photons, but multiphoton ionization can cause neutral cluster fragmentation and thus, loss of original cluster mass identity. Single photon ionization near threshold is the best approach, but these clusters generally have ionization energies greater than 7–8 eV and single photon energies above this energy are difficult to generate at reasonable intensities (greater than 10<sup>11</sup> photons/pulse).

The problem of cluster detection without interference from, or confusion generated by, parent neutral cluster fragmentation can be addressed in two ways: covariance mapping of the mass spectral data,<sup>2</sup> and single photon ionization near threshold with vacuum ultraviolet photons. In this work we have chosen the latter approach, employing 118 nm (10.5 eV) photons generated by the following chain of nonlinear optical events:<sup>3</sup>



The full process is the generation of the ninth harmonic of the Nd/YAG laser fundamental output. The overall conver-

sion involves the seeded output of  $\approx 800$  mJ/pulse (8 ns pulsewidth) at 1064 nm to yield the 118 nm output at  $\approx 0.5 \mu\text{J/pulse}$  ( $\sim 10^{11}$  photons/pulse) with a pulsewidth of  $\approx 10$  ns.

In this report we present the mass spectra of neutral iron oxide clusters obtained at 355, 193, 118 nm laser ionization, and through the analysis of mass spectral linewidths, laser power dependence, and relative intensities of spectral features, the neutral cluster iron oxide distribution for different experimental conditions is determined.

The 118 nm (10.5 eV) photons have two distinct advantages over other laser wavelengths that can be employed for the cluster ionization process: (1) a single 10.5 eV photon is energetic enough to ionize any iron oxide neutral cluster; and (2) at 10<sup>11</sup>–10<sup>12</sup> photons/pulse at 118 nm, the probability that any cluster will absorb more than one photon is vanishingly small.

In this work, we determine that the most stable and abundant neutral clusters are of the forms Fe<sub>m</sub>O<sub>m</sub>, Fe<sub>m</sub>O<sub>m+1</sub>, and Fe<sub>m</sub>O<sub>m+2</sub>. As *m* increases, the more oxygen rich clusters tend to dominate the distribution for a given value of *m*. These changes occur about *m* ~ 10 for Fe<sub>m</sub>O<sub>m+1</sub> clusters and about *m* ~ 18 for Fe<sub>m</sub>O<sub>m+2</sub>.

### II. EXPERIMENTAL PROCEDURES

Since the overall experimental system has been described in detail elsewhere,<sup>2–4</sup> only a general outline of the experimental scheme will be presented in this report. The new features of these studies relevant to the generation of the 118 nm ionization laser light will be presented here in detail.<sup>3</sup>

Neutral clusters of iron oxide are generated and cooled in a supersonic expansion of He gas. The clusters are synthesized by laser ablation of an iron metal foil. The iron metal plasma plume from the ablation process interacts with the  $\approx 1\%$   $\text{O}_2/99\%$  He gas that passes over the ablation point, thus generating  $\text{Fe}_m\text{O}_n$  clusters. The expansion gas/cluster mixture passes into a vacuum system that contains a time-of-flight mass spectrometer (TOFMS). Neutral clusters are ionized by laser radiation (355, 193, or 118 nm) and detected and characterized in the TOFMS.

The 118 nm radiation is generated by a frequency tripling gas cell (269 mm long and 35 mm in diameter) into which 355 nm pulsed, seeded Nd/YAG tripled laser radiation is focused. The tripling cell is sealed at the 355 nm input end by a suprasil quartz window and at the 118 nm output end by a  $\text{MgF}_2$  plano-convex lens having a focal length of 150 mm at 250 nm (JANOS, A0604V115). The tripling cell contains a mixture of Xe and Ar gas. Under our conditions ( $\leq 24$  mJ/pulse at 355 nm), the optimal conversion efficiency of 355 nm to 118 nm radiation is achieved at a mixing ratio of Xe/Ar  $\sim 1/10$  and at a total pressure of  $\sim 200$  Torr. The total pressure in the cell is measured by an absolute pressure gauge.

The focal lengths of the  $\text{MgF}_2$  lens at 118 nm and 355 nm are very different ( $f=84$  mm@118 nm and  $f=151$  mm@355 nm); the cell is attached to the mass spectroscopy chamber such that the 118 nm focus is at the ionization region and while the residual 355 nm beam is defocused at the molecular beam position in the ionization region. The  $\text{MgF}_2$  lens is located  $\sim 300$  mm from the ionization region. The 355 nm laser light is focused at about 115 mm from the  $\text{MgF}_2$  lens by an  $f=25$  mm@355 nm quartz lens. The pair of lenses gives a focus of the 118 nm light at the ionization region (focal size  $\sim 25$   $\mu\text{m}$  for a Gaussian laser beam) while the 355 nm laser light is diverged to about 7–8 mm at this point. This ionization system is tested with a few ppm NO in He in a supersonic expansion. NO has an ionization energy of 9.264 eV and can be ionized by single photon ionization with a 118 nm source. The focus and intensity of the 118 nm beam is checked with NO and found to generate a strong signal ( $\approx 3$  V on an oscilloscope directly connected to the microchannel plate detector) with a  $\approx 10$  ns linewidth. With the cell pumped out so that only 355 nm laser light passes into the ionization region, the NO signal is  $< 10$  mV. This shows that the defocused 355 nm beam does not hit any metal in the ionization region that will generate electrons and could still cause ionization.

If the clusters do not fragment ( $\tau_{\text{frag}} > 2$   $\mu\text{s}$ ) or if they fragment very rapidly ( $\tau_{\text{frag}} < 1$  ns), the linewidth of the features observed in the mass spectrum of a sample is related to the laser pulsewidth in time and the focal size of the laser in the ionization region. The laser pulsewidths are all about 10 ns for a seeded laser (355 and 118 nm) or the excimer (193 nm), but for an unseeded Nd/YAG laser, the output at all wavelengths consists of a series of  $\sim 100$  ps wide, mode locked, intense pulses that vary in time from pulse to pulse with an average  $\sim 10$  ns Gaussian-type envelope. Thus, the 118 nm ionization mass spectral linewidths with no cluster fragmentation should be  $\approx 10$  ns for a seeded laser and could

be  $\approx 2$  ns (governed by the sample time of the oscilloscope) on a shot-to-shot basis. Data are collected and stored for these spectra on a shot-to-shot basis with an averaged spectrum computed after a complete run of  $\approx 2000$  laser shots.<sup>2,5</sup> For 193 nm ionization, the laser is focused to about  $0.5 \times 2$  mm spot size so in this case, without fragmentation, a  $\approx 10$  ns averaged spectral linewidth can also be anticipated. On the other hand, for any ionization by 355 nm laser radiation, mass spectral linewidths should be at least  $\approx 25$  ns wide due to the spatial variation of the birth positions of the (unfragmented) ions. The number of 118 nm photons/pulse generated from a 355 nm input beam is calculated to be  $4 \times 10^{11}$  photons at a 355 nm pulse energy of 23.5 mJ. We have assumed that the conversion efficiency of 355–118 nm is about  $10^{-5}$ .<sup>3</sup> The experimental conditions for the various spectra presented in this report can be different in order to emphasize different components of the mass distribution. Thus, different mass features will appear more prominently, depending on ionization laser beam size, voltages on mass spectrometer deflection plates, growth conditions, etc.

### III. RESULTS

Following the laser ablation of iron foil with a 532 nm, 10 ns pulsed, doubled Nd/YAG laser at  $\approx 6$  mJ/pulse in the presence of 0.75%  $\text{O}_2$  in 20 psig He, the various concentrations of neutral clusters are generated and cooled through an adiabatic expansion into the vacuum. In this study, three different ionization laser wavelengths are employed for multiphoton (355 nm and 193 nm) and single photon (118 nm) ionization processes. Through these three different neutral cluster ionization methods, the neutral cluster distribution can be determined. Figures 1(a) and 1(b) show the mass spectra obtained at ionization wavelengths of 355 nm (23.5 mJ/pulse) and 193 nm (0.8 mJ/pulse) for an ablation laser energy of 6.2 mJ/pulse. At 193 nm, in agreement with our previous report,<sup>4</sup>  $\text{Fe}_m\text{O}_n^+$  cluster ions with  $n=m$  and  $m+1$  are the most prominent features, with the more oxygen rich clusters appearing as  $m$  increases. Oxygen deficient clusters,  $\text{Fe}_m\text{O}_{m-1}^+$  and  $\text{Fe}_m\text{O}_{m-2}^+$  also can be observed under 193 nm ionization [Fig. 1(b)]. For 355 nm ionization, oxygen deficient clusters are not readily observed. In this figure, the experimental conditions are adjusted to generate  $\text{Fe}_m\text{O}_n$ ,  $m < 20$ .

With 118 nm ionization laser radiation, the mass spectrum of  $\text{Fe}_m\text{O}_n^+$  changes significantly. In Fig. 1(c), the 355 nm laser energy is 23.5 mJ/pulse. Each mass feature generated at 118 nm ionization is much narrower compared to those generated at 193 nm. One can also observe (especially for  $\text{Fe}_m\text{O}_m^+$ ,  $m \leq 9$  and  $\text{Fe}_m\text{O}_{m+1}^+$ ,  $m \leq 5$ ) the presence of the iron isotopes. The ionization process for 118 nm radiation is by single photon, and for 355 nm and 193 nm, the process is multiphoton. Note that, in most instances ( $\text{Fe}_2\text{O}_1^+$  is an exception, but see below), the intense features are of the form  $\text{Fe}_m\text{O}_m^+$ ,  $\text{Fe}_m\text{O}_{m+1}^+$ , and  $\text{Fe}_m\text{O}_{m+2}^+$  (except for 355 nm ionization). This fact alone strongly suggests that these cluster series,  $\text{Fe}_m\text{O}_m^+$ ,  $\text{Fe}_m\text{O}_{m+1}^+$ , and  $\text{Fe}_m\text{O}_{m+2}^+$ , are the most abundant ones for the neutral cluster distribution. Linewidth data (discussed below) will further substantiate this conclu-

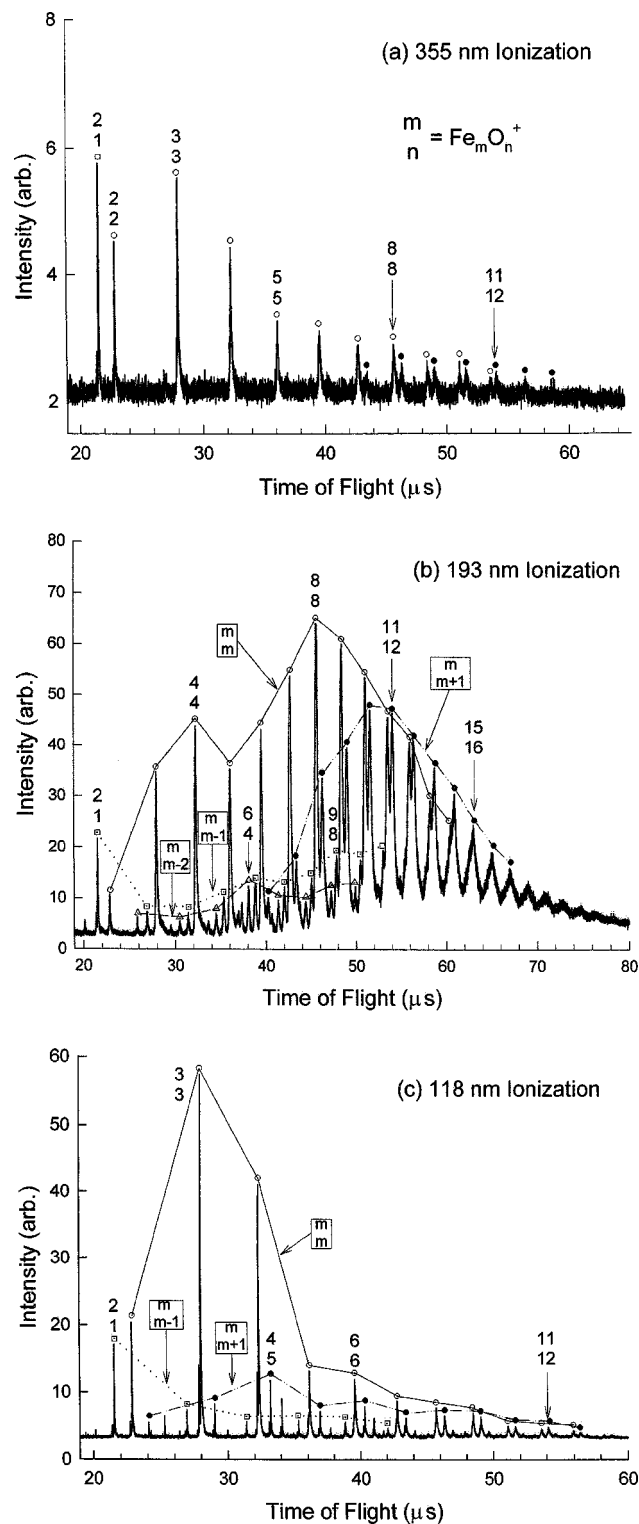


FIG. 1. TOF mass spectra of iron oxide clusters ionized by three different ionization wavelengths, (a) 355 nm, (b) 193 nm, and (c) 118 nm (stagnation pressure: 20 psig, ablation laser pulse energy: 6.2 mJ/pulse). The average ionization laser pulse energies of 355 and 193 nm are 34.5 and 0.8 mJ/pulse. The observed iron oxide cluster ions of the form  $\text{Fe}_m\text{O}_n^+$  are labeled as  $\binom{m}{n}$ . The significant change in the mass spectrum represents the variation of the ionization processes. The experimental conditions are set for these spectra to enhance intensity of small clusters. Additionally, resolution at high mass ( $m > 15$ ) is degraded so the  $\text{Fe}_m\text{O}_{m+1}$  and  $\text{Fe}_m\text{O}_{m+2}$  features overlap due to the laser beam focus. Each peak is classified by symbols according to the number of Fe and O atoms: open triangles,  $\text{Fe}_m\text{O}_{m-2}^+$ ; open squares,  $\text{Fe}_m\text{O}_{m-1}^+$ ; open circles,  $\text{Fe}_m\text{O}_m^+$ ; closed circles,  $\text{Fe}_m\text{O}_{m+1}^+$ .

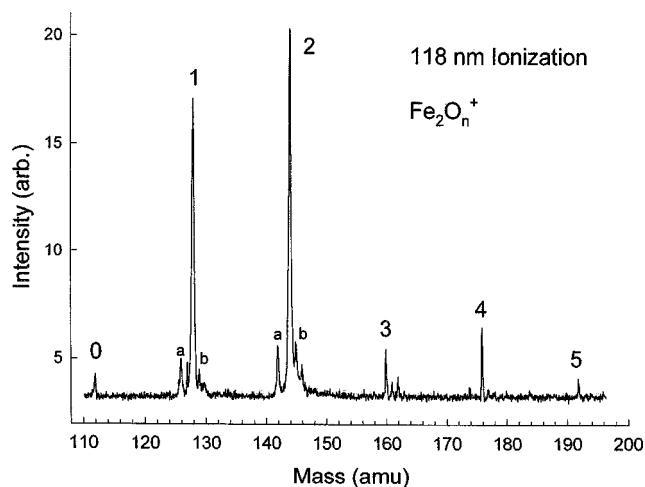


FIG. 2. Expanded portion of the mass spectrum of Fig. 1(c) for the region of cluster ion containing two Fe atoms in iron oxide cluster ions,  $\text{Fe}_2\text{O}_n^+$ . The peaks labeled as a and b next to the major peaks are due to the iron isotopes (see text for details).

sion. Finally, note that the 118 nm ionization spectrum of Fig. 1(c) gives the intensity distribution of the clusters as generally decreasing with cluster size. This is to be expected for a growth pattern and may well truly reflect the neutral cluster concentration distribution in the beam.

New features in the mass spectrum of  $\text{Fe}_m\text{O}_n$  are observed at 118 nm ionization, not found for 193 nm ionization. A part of the lower cluster range of the 118 nm ionization spectrum is displayed in Fig. 2; the observed cluster spectrum for  $\text{Fe}_2\text{O}_n^+$  contains six features from  $\text{Fe}_2^+$  to  $\text{Fe}_2\text{O}_5^+$ . The highly oxygen rich species  $\text{Fe}_2\text{O}_4^+$  and  $\text{Fe}_2\text{O}_5^+$  are not observed with 193 nm ionization. The features labeled a and b in Fig. 2 correspond to  $^{54}\text{Fe}^{56}\text{FeO}_n^+$  and  $^{56}\text{Fe}^{57}\text{FeO}_n^+$ , respectively. Note that  $\text{Fe}_2\text{O}_3^+$ ,  $\text{Fe}_2\text{O}_4^+$ , and  $\text{Fe}_2\text{O}_5^+$  features are very narrow, roughly one-half the width of the more intense  $\text{Fe}_2\text{O}_1^+$  and  $\text{Fe}_2\text{O}_2^+$  features. Again, line-width data for the various mass spectra will be presented below.

The cluster ion distribution observed in the mass spectrum at 118 nm ionization depends on several experimental parameters, such as ablation laser power, and the relative timing of the nozzle expansion, ablation laser firing, and ionization laser firing. If the effect of 355 nm ionization can be separated from that of 118 nm ionization, the 118 nm ionization spectrum could well reflect the true neutral cluster distribution in the absence of fragmentation due to the ionization processes. This point will be discussed later in the next section following presentation of the detailed linewidth data. Figure 3 shows the mass spectrum of the  $\text{Fe}_m\text{O}_n$  clusters under exactly the same conditions as presented in Figs. 1(c) but with the mass spectrometer  $x, y$  deflection plate voltages (these plates are parallel to the long, 1.5 m  $z$ -axis of the flight tube), which correct for motion of the created ions not in the direction of flight to the mass detector microchannel plate, set to maximize the intensity of larger clusters. These steering or deflector plates cause small changes in the peak intensity ratios for iron oxide clusters with the same number of iron atoms but different numbers of oxygen atoms. This ob-

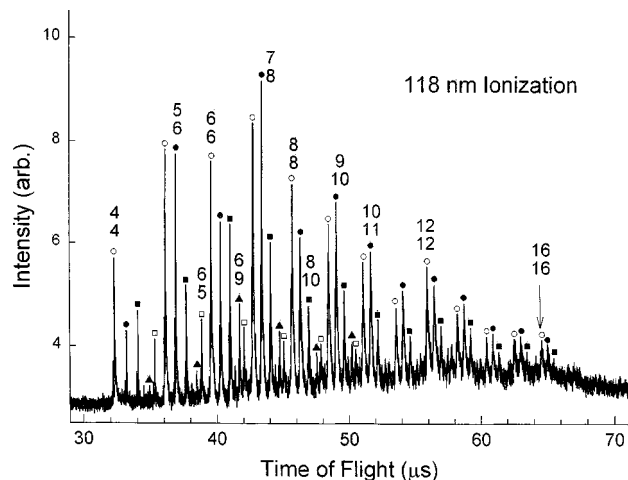


FIG. 3. TOF mass spectrum obtained at 118 nm under identical conditions like Fig. 1(c) except that the deflection voltages of mass spectrometer and the timing between nozzle and ablation and ionization lasers are changed to optimize the high clusters. The cluster ions  $\text{Fe}_m\text{O}_n^+$  are labeled as  $mn$ . Each peak is also classified by symbols according to the number of Fe and O atoms; open circle,  $\text{Fe}_m\text{O}_m^+$ ; closed circle,  $\text{Fe}_m\text{O}_{m+1}^+$ ; closed square,  $\text{Fe}_m\text{O}_{m+2}^+$ ; open square  $\text{Fe}_m\text{O}_{m-1}^+$ ; closed triangle,  $\text{Fe}_m\text{O}_{m+3}^+$ .

ervation probably implies that different parts of the molecular beam are being accessed as the deflector voltages are varied and that the beam is not homogeneous in  $\text{Fe}_m\text{O}_n$  clusters due to growth characteristics and velocity skip for clusters of different sizes. Thus, the actual neutral cluster distribution in the expansion beam is a composite of the various individual spectra obtained at each deflector voltage setting and for each ionization laser/nozzle/ablation laser timing delay. A comparison of several spectra can give a qualitative estimate of the overall distribution of clusters. The general series intensity patterns, as described herein, can be well resolved through this comparison. In this spectrum, the intensity of oxygen deficient clusters is significant, even at low cluster sizes (e.g.,  $\text{Fe}_6\text{O}_5^+$ ,  $\text{Fe}_5\text{O}_4^+$ ).

Figure 4 presents an expanded portion of the 193 nm and 118 nm cluster spectra for the region  $\text{Fe}_5\text{O}_7^+$  through  $\text{Fe}_8\text{O}_{10}^+$ . As mentioned earlier, the common feature of these two mass spectra is the predominant formation of iron oxide clusters  $\text{Fe}_m\text{O}_m^+$ ; for example,  $\text{Fe}_6\text{O}_6^+$ ,  $\text{Fe}_7\text{O}_7^+$ , and  $\text{Fe}_8\text{O}_8^+$ . Other features in the 193 nm spectrum include the oxygen deficient series  $\text{Fe}_m\text{O}_{m-1,2,3}^+$ , whereas the 118 nm spectrum shows strong features for the oxygen rich series  $\text{Fe}_m\text{O}_{m+1,2,3}^+$ . For 118 nm ionization, the oxygen deficient series is weak, and for 193 nm ionization, the oxygen rich series is weak. The point to note from these results and comparisons is that the 118 nm ionization spectrum is probably free or close to free of fragmentation.

Figure 5 presents the time-of-flight mass spectra of iron oxide clusters obtained by 193 and 118 nm ionization at low pulse energies. The ionization pulse energy dependence behavior at 193 nm ionization is quite different from that at 118 nm ionization. Reducing the 193 nm ionization average pulse energy leads to a wider distribution of iron oxide cluster ions with a shift of the most intense features to higher cluster mass, and an absence of any cluster ions below  $\text{Fe}_8\text{O}_9^+$ . In contrast, at low 118 nm ionization average pulse energy (low

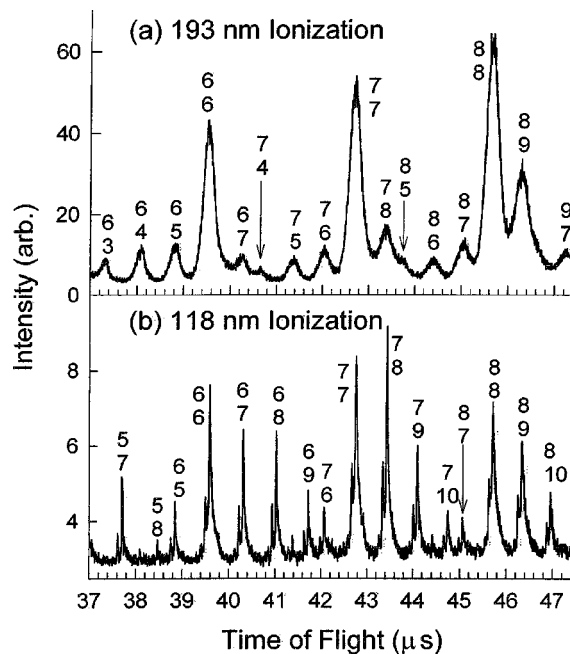


FIG. 4. Expanded portions of the mass spectra of Figs. 1(b) and 3 for the region of  $\text{Fe}_3\text{O}_4^+$  through  $\text{Fe}_9\text{O}_7^+$  clusters. Spectra (a) and (b) are obtained with 0.8 mJ of 193 nm light for ionization and 118 nm light for ionization generated by 23.5 mJ of 355 nm light, respectively. The clusters  $\text{Fe}_m\text{O}_n^+$  are labeled as  $mn$ .

355 nm pulse energy), higher mass iron oxide clusters are lost from the mass spectrum, and only clusters smaller in size than  $\text{Fe}_5\text{O}_6^+$  are observed. Changes in the 118 nm spectra with ionization laser power suggest that small neutral clusters are more abundant than large ones. The 193 nm cluster ionization behavior suggests that clusters  $\text{Fe}_m\text{O}_n$ ,  $m \leq 7$ , have high ionization energies and/or small cross sections for multiphoton absorption. Taken together, these results imply that fragmentation of clusters is local rather extensive, such that,  $\text{Fe}_m\text{O}_n \rightarrow \text{Fe}_m\text{O}_{n-1,2}$  or  $\text{Fe}_{m-1,2}\text{O}_n$  or  $\text{Fe}_{m-1}\text{O}_{n-1}$ , but

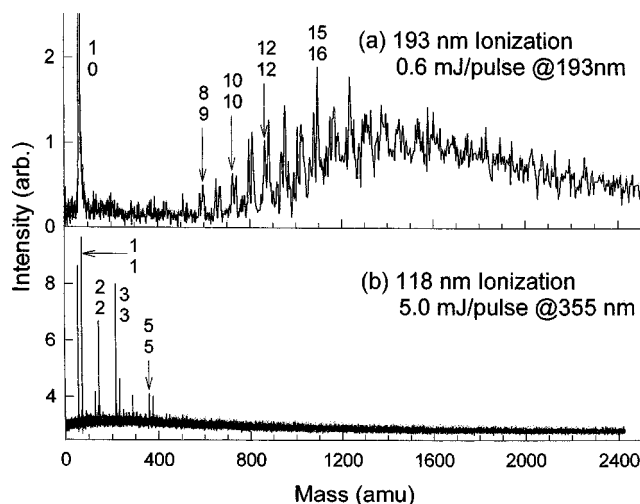


FIG. 5. TOF mass spectra of iron oxide clusters ionized at (a) 193 nm (average ionization pulse energy: 0.6 mJ/pulse and ablation pulse energy: 2.5 mJ/pulse) and (b) 118 nm (pulse energy of 355 nm: 5.0 mJ/pulse and ablation pulse energy: 6.3 mJ/pulse) in low laser average pulse energy region. Some peaks are labeled as  $mn$  for  $\text{Fe}_m\text{O}_n^+$ .

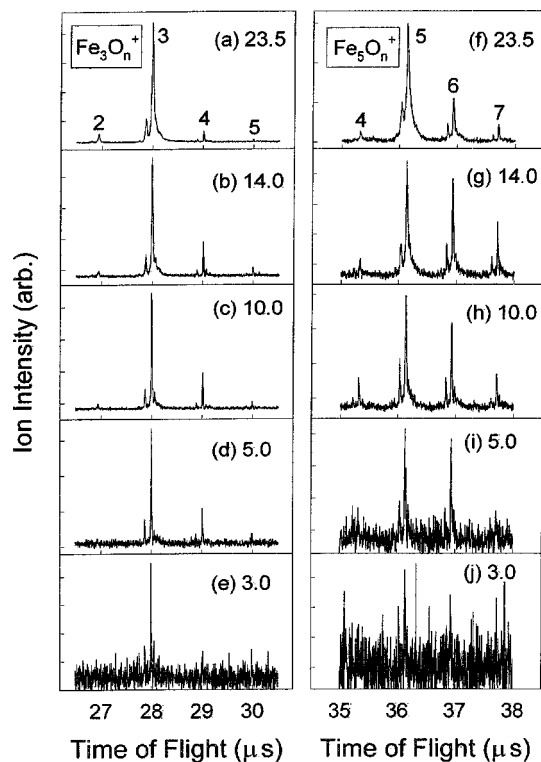


FIG. 6. TOF mass spectra of  $\text{Fe}_3\text{O}_n^+$  ( $n=2-5$ ) and  $\text{Fe}_5\text{O}_n^+$  ( $n=4-7$ ) cluster ions at the 118 nm ionization as a function of the pulse energy of 355 nm (at the range 3.0–23.5 mJ/pulse) for 118 nm generation. All y axes are scaled to the highest peaks, such as  $\text{Fe}_3\text{O}_3^+$  and  $\text{Fe}_5\text{O}_3^+$ .

not so extensive as to generate small cluster ions from large neutral clusters. Cluster fragmentation will be discussed further in the next section.

The 118 nm photons/pulse is never higher than  $\sim 4 \times 10^{11}$  (at 23.5 mJ/pulse, 355 nm) and thus, the possibility of multiphoton effects from these photons is negligible. Nonetheless, since the conversion efficiency of 355 nm photons to 118 nm photons is  $\approx 10^{-5}$ , the unconverted 355 nm light may be a factor in the ionization process of iron oxide clusters for the assumed 118 nm ionization process. Figure 6 seems to show the effect of 355 nm radiation on the ionization of iron oxide clusters for 118 nm radiation. The intensity axes of these spectra (a–j) are all normalized to the highest intensity feature in the spectrum for each  $\text{Fe}_3\text{O}_n^+$  and  $\text{Fe}_5\text{O}_n^+$  cluster. Note two features of these spectra: (1) as the 355 nm laser energy/pulse is reduced, the features become sharper; and (2) oxygen rich cluster relative intensity increases, and oxygen poor cluster relative intensity decreases, as laser pulse energy is lowered. Thus, these comparisons suggest that the  $\text{Fe}_m\text{O}_m$ ,  $\text{Fe}_m\text{O}_{m+1,2}$  are members of the neutral cluster distribution and not cluster ions associated with fragmentation. The oxygen deficient clusters may well be generated by a fragmentation process related to multiphoton 355 nm radiation absorption or 118 nm plus 355 nm radiation absorption.

To obtain a quantitative description of the spectral line-widths for the observed mass spectra, Gaussian distributions

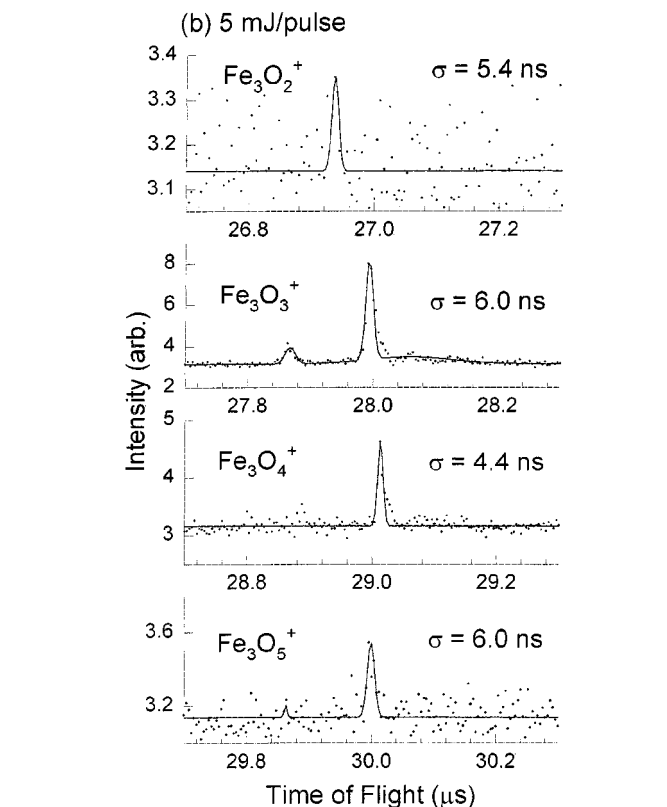
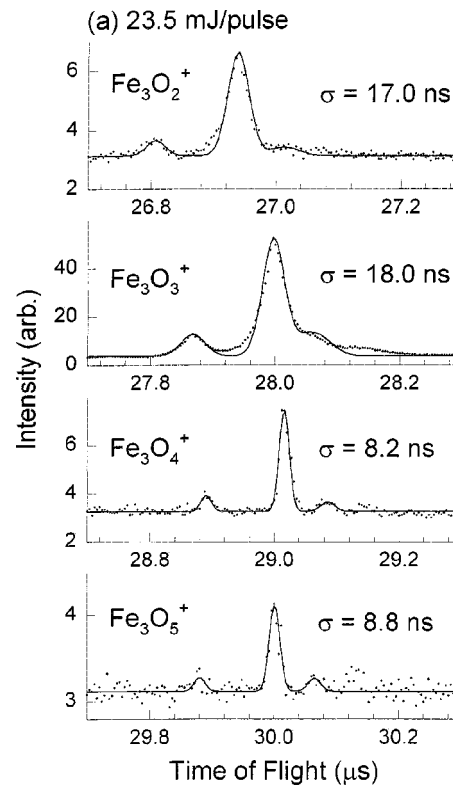


FIG. 7. Gaussian widths,  $\sigma$ , of  $\text{Fe}_3\text{O}_n^+$  cluster ion peaks at two different pulse energies of 355 nm light for the generation of 118 nm light; (a) 23.5 mJ/pulse and (b) 5 mJ/pulse. The fitted line shape is the solid line.

of peak intensity are fitted to the measured peaks of  $\text{Fe}_3\text{O}_n^+$  cluster ions, which are observed to be the most intense features of the 118 nm ionization spectrum.

The half linewidth is calculated from

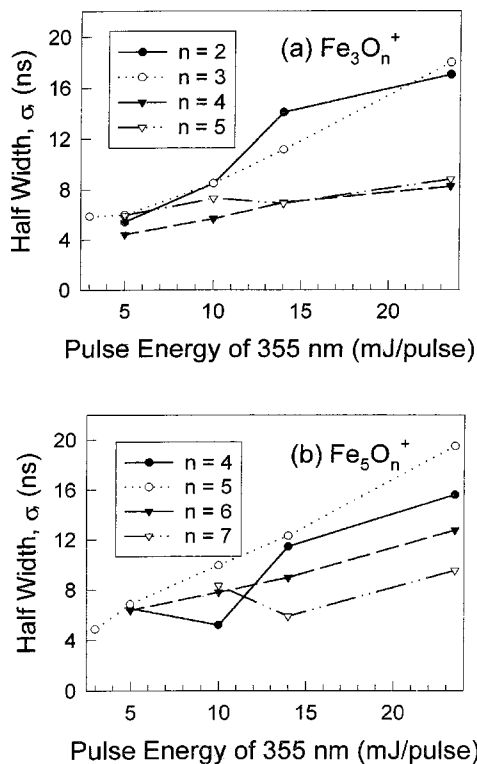


FIG. 8. Gaussian widths of (a)  $\text{Fe}_3\text{O}_n^+$  and (b)  $\text{Fe}_5\text{O}_n^+$  cluster ions as a function of pulse energy of 355 nm light for the generation of 118 nm light.

$$I = a \exp\left[-\frac{1}{2}\left(\frac{t_1 - t_0}{\sigma}\right)^2\right] + a' \exp\left[-\frac{1}{2}\left(\frac{t'_1 - t'_0}{\sigma'}\right)^2\right] + \dots,$$

in which  $I$  is the observed ion intensity,  $a$  is the peak height,  $t_0$  is the center of the peak, and  $\sigma$  is the “Gaussian width” of the peak. The first term in the Gaussian line shape function corresponds to the spectrum component created by one ionization wavelength (e.g., 118 nm) and the second term corresponds to the spectrum component created by a second ionization wavelength (e.g., 355 nm) if present.  $\sigma$  can be converted in the full width of the feature at half maximum intensity (FWHM)  $\Delta t_{1/2}$  with the conversion constant 2.355 ( $\Delta t_{1/2} = 2\sqrt{2} \ln 2 \sigma$ ). The fitted curves are shown in Fig. 7 as a red line. The small features next to the most intense features in the spectra are iron isotopic peaks. The values of  $\sigma$  in Fig. 7 are given for the  $^{65}\text{Fe}_3\text{O}_n^+$  clusters. Note that the larger, higher mass clusters have smaller linewidths at the higher ionization pulse energy. Thus, the contribution of 355 nm absorption and subsequent cluster ion fragmentation to the linewidths of the lower mass cluster ions (loss of oxygen from higher mass ions) is observed for the high energy/pulse ionization laser condition [Fig. 7(a)]. On the other hand, at low ionization laser energy/pulse [Fig. 7(b)], all the  $\text{Fe}_3\text{O}_n^+$  features have roughly the same linewidth with the obvious suggestion being that fragmentation is no longer occurring for these conditions. In fact, even for cluster systems that do not undergo fragmentation,<sup>2</sup> and for molecules that do not undergo fragmentation,<sup>6</sup> these are about as narrow as any mass spectral features observed in this apparatus. Note that the  $\text{Fe}_3\text{O}_4^+$  and  $\text{Fe}_3\text{O}_5^+$  mass spectral linewidths obtained at 23.5 mJ/pulse of 355 nm laser ionization energy [Fig. 7(a)]

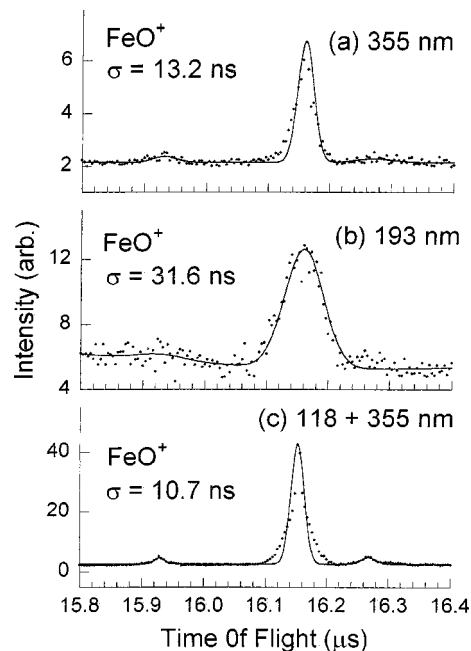


FIG. 9. Gaussian widths of  $\text{FeO}^+$  ions at three different ionization wavelengths. The laser energy is (a), (c) 24 mJ/pulse at 355 nm and (b) 0.75 mJ/pulse at 193 nm. The fitted line shape is the solid line.

are roughly 50% larger than those obtained at 5 mJ/pulse 355 nm laser ionization energy [Fig. 7(b)]. This linewidth difference with 355 nm ionization laser power could be due to a small amount of fragmentation of the form  $\text{Fe}_4\text{O}_{4.5}^+ \rightarrow \text{Fe}_3\text{O}_{4.5}^+$  following absorption of one 118 nm photon and  $n$  ( $\geq 1$ ) 355 nm photons by the  $\text{Fe}_4\text{O}_{4.5}$  neutral clusters.

Figure 8 shows plots of Gaussian widths  $\sigma$  as a function of 355 nm laser energy/pulse for the 118 nm ionization process for the two cluster species series,  $\text{Fe}_3\text{O}_n^+$  and  $\text{Fe}_5\text{O}_n^+$ . Figure 9 shows the spectra for  $\text{FeO}^+$  at different ionization laser wavelengths. The line shape for 118 nm+355 nm radiation is not simple and suggests that two component ionization processes contribute to the line intensity and shape. More fragmentation is found for this cluster at 193 nm ionization than at 355 nm ionization. The 118 nm contribution can be suggested to be due to a single photon/nonfragmentation process. Similar behavior can be observed for  $\text{Fe}_3\text{O}_3^+$  in Fig. 10. The  $\text{FeO}^+$  118 nm+355 nm ionization feature is deconvoluted in Fig. 11 such that the 118 nm single photon contribution yields a Gaussian width of  $\sigma = 3.4$  ns, while the 355 nm Gaussian width is  $\sigma = 20.4$  ns, and a combined Gaussian width of  $\sigma = 10.7$  ns can be calculated.

#### IV. DISCUSSION

The main results from the last section can be generalized as follows: (1) at three different wavelengths for ionization, the most intense features in the TOFMS of neutral iron oxide clusters are of the form  $\text{Fe}_m\text{O}_m^+$ ; (2) iron oxide clusters containing excess oxygen (e.g.,  $\text{Fe}_m\text{O}_{m+1,2}^+$ ) are observed in the 118 nm ionization cluster spectra with good intensity and narrow linewidths, while the 193 nm ionization spectra display both oxygen rich (e.g.,  $\text{Fe}_m\text{O}_{m+1}$  and  $\text{Fe}_m\text{O}_{m+2}$  at  $m > 12$ ) and oxygen deficient clusters (e.g.,  $\text{Fe}_m\text{O}_{m-1,2,3}^+$   $m$

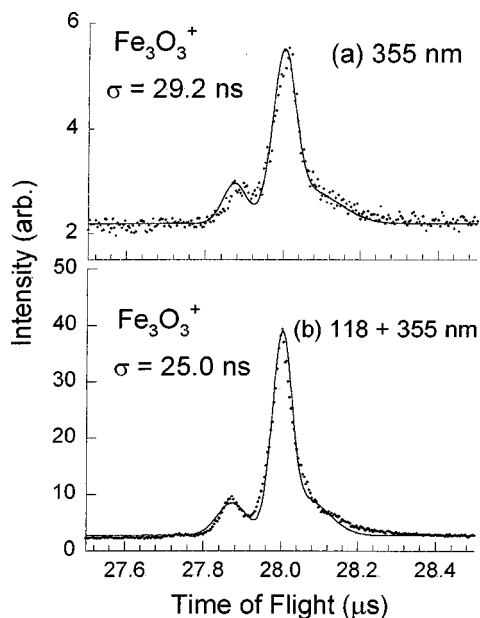


FIG. 10. Gaussian widths of  $\text{Fe}_3\text{O}_3^+$  cluster ions at two different ionization wavelengths. The laser energy is 23.5 mJ/pulse at 355 nm. The fitted line shape is the solid line.

<12) with good intensity and broad linewidths; (3) the ionization laser pulse energy affects the obtained cluster distributions differently for 193 nm and 118 nm ionization—as the ionization laser energy/pulse decreases, the distribution of iron oxide clusters narrows toward the small cluster at 118 nm ionization, while it becomes broader and emphasizes larger clusters for 193 nm ionization; and (4) narrow and anticipated linewidths ( $\Delta t_{1/2} = 2.355 \text{ ns} \sim 10 \text{ ns}$ ) for all features in a mass spectra are only achieved for 118 nm ionization.

### A. Neutral cluster distribution

Even for 355 and 193 nm multiphoton ionization of the neutral cluster distribution, which we know causes cluster fragmentation based on linewidth data, the predominate features in the mass spectrum of iron oxide clusters are of the form  $\text{Fe}_m\text{O}_m^+$ ,  $\text{Fe}_m\text{O}_{m+1.2}^+$ . This is also true for 118 nm ion-

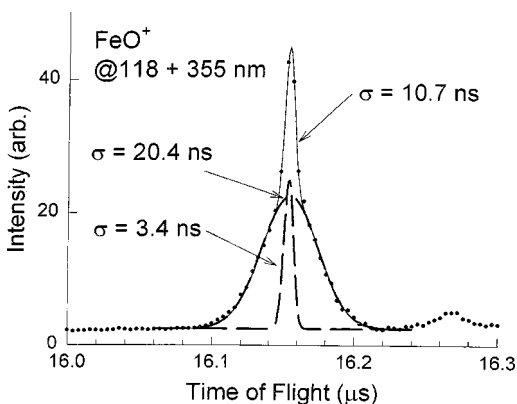


FIG. 11. Deconvolution of  $\text{FeO}^+$  Gaussian width. The laser energy is 23.5 mJ/pulse at 355 nm. The fitted line shape is in red for the 118 nm ionization component and blue for the 355 nm ionization component. The overall fitted line shape is the thin solid line.

ization for which the linewidth results, ionization energies, and photon densities all suggest single photon, nonfragmenting ionization occurs at this ionization wavelength. Thus, we can conclude that the thermodynamically most stable neutral clusters are of the form  $\text{Fe}_m\text{O}_m$  with  $\text{Fe}_m\text{O}_{m+1.2}$  clusters also present in the beam at large concentrations. Clusters of the form  $\text{Fe}_m\text{O}_{m-1.2}$  are observed at 118 nm ionization but seem to be less abundant than the others. The 118 nm ionization intensities do not necessarily represent the “true” neutral cluster distribution because absorption cross section and possible fragmentation of large clusters with low ionization energies can distort the actual concentrations of neutral clusters. Nonetheless, one can be confident in the general trends suggested.

The present generation techniques for the clusters seem to emphasize small clusters, but the distribution stretches to roughly  $m = 25\text{--}30$  for  $\text{Fe}_m\text{O}_n$ . For masses much larger than these, the TOFMS used in these experiments begins to lose resolution for  $\text{Fe}_m\text{O}_m$  and  $\text{Fe}_m\text{O}_{m\pm 1}$  at low signal/noise ratio.

The reason for the cluster distribution changing oppositely with low laser pulse energy for 118 nm and 193 nm ionization is probably twofold. The ionization energy of  $\text{FeO}$  and  $\text{FeO}_2$  are 8.9 eV and 9.5 eV, respectively.<sup>7</sup> Thus, 193 nm ionization is multiphoton only, and as this laser power decreases, the multiphoton process is becoming less likely. Additionally, the cross section for multiphoton absorption is smaller for small clusters than for large clusters due to the reduced cluster density of states. On the other hand, for 118 nm ionization, the cross section may be more or less constant for all clusters within the continuum absorption, but for low photon densities ( $10^{10}\text{--}10^{11}$  photons/pulse) and low cluster concentrations (e.g., for  $m > 10$ ), the observed cluster ion distribution narrows toward small clusters. Eventually, for large enough  $m$ , the 193 nm ionization process could be energetically single photon, but cross sections for resonant multiphoton absorption in both the neutral and the ion may still enhance 193 nm ionization fragmentation processes. The Fe–Fe and Fe–O bond strengths are estimated as 1–4.2 and 4.3 eV, respectively.<sup>7</sup>

### B. Fragmentation mechanism

The fragmentation reaction must occur in  $\leq 1 \mu\text{s}$  in the TOFMS ionization region, to be observed as a change in mass. Since intramolecular vibrational redistribution (IVR) and vibrational predissociation (VP) depend oppositely on density of states (that is, vibronic relaxation is slow for small clusters and fast for large clusters, but dissociation is fast for small clusters and slow for large clusters), some fragmentation can go unobserved for near threshold ionization. The combined cluster fragmentation times (including both IVR and VP processes) can be greater than  $1 \mu\text{s}$ , especially for large clusters.

These results tend to imply that the cluster fragmentation observed at 355 and 193 nm ionization wavelengths is most likely local. The idea of “local fragmentation” is that  $\text{Fe}_m\text{O}_{m+1} \rightarrow \text{Fe}_m\text{O}_m^+$  or  $\text{Fe}_m\text{O}_{m-1}^+$ , ... and  $\text{Fe}_m\text{O}_m \rightarrow \text{Fe}_m\text{O}_{m-1}^+$  or  $\text{Fe}_m\text{O}_{m-2}^+$ , ... occurs, but that  $\text{Fe}_m\text{O}_{m+1} \rightarrow \text{Fe}_{m-x}\text{O}_{m+1-y}^+$  does not occur. This mechanism can be

suggested based on the observed linewidth data: that is,  $\text{Fe}_m\text{O}_{m+1,2}^+$  features tend to be narrower than  $\text{Fe}_m\text{O}_{m-1,2}^+$  features. If loss of iron did occur upon ionization, then the  $\text{Fe}_m\text{O}_{m+1,2}^+$  cluster could arise from  $\text{Fe}_{m+1}\text{O}_{m+1,2}$  clusters and the  $\text{Fe}_m\text{O}_{m+1,2}^+$  features would have large linewidths just as the  $\text{Fe}_m\text{O}_{m-1,2}^+$  do.

## V. CONCLUSIONS

Through a comparison of cluster ion distribution and TOFMS signal linewidths observed for 355 nm, 193 nm, and 118 nm laser ionization, the neutral iron oxide cluster distribution is characterized for given conditions of laser ablation of the metal, oxygen concentration, and supersonic expansion pressures. We conclude from these studies the following:

- (1) For clusters with fewer than 10 iron atoms, the most stable neutral clusters are of the form  $\text{Fe}_m\text{O}_m$  ( $m \leq 10$ );
- (2) For larger clusters,  $m \geq 10$ , oxygen rich clusters begin to appear with significant intensity,  $\text{Fe}_m\text{O}_{m+1,2}$ ;
- (3) Clusters of the form  $\text{Fe}_m\text{O}_{m-1,2}$  also can be observed but are generally less abundant than the others;
- (4) Cluster features have Gaussian widths as small as  $\sigma \sim 4$  ns ( $\Delta t_{1/2} \sim 10$  ns) for 118 nm ionization; and
- (5) Linewidths arise from laser spot size in the ionization region, laser pulsewidth, and fragmentation of neutral clusters.

We are now in the process of studying reactions of these neutral clusters with small gas phase molecules such as  $\text{NO}_x$ , CO,  $\text{SO}_2$ ,  $\text{NH}_3$ ,  $\text{H}_2\text{O}$ , and others.

## ACKNOWLEDGMENTS

This research is supported in part by grants from Philip Morris USA and the U.S. Department of Energy. We also thank Professor S. R. Leone for a number of practical suggestions concerning 118 nm light generation.

- <sup>1</sup>(a) E. L. Mutttert, T. N. Rodin, E. Brand, C. F. Brucker, and W. Pretzer, *Chem. Rev. (Washington, D.C.)* **79**, 91 (1979); (b) K. Eller and H. Schwarz, *ibid.* **91**, 1121 (1991), and references therein to earlier work; (c) D. Schröder and H. Schwarz, *Angew. Chem., Int. Ed. Engl.* **34**, 1973 (1995); (d) G. Ertl and H. J. Freund, *Phys. Today* **52**, 32 (1999); (e) P. A. Hackett, S. A. Mitchell, D. M. Rayner, and B. Simard, in *Metal-Ligand Interactions*, edited by R. Russo and D. R. Salahub (Kluwer, Amsterdam, 1996), p. 289.
- <sup>2</sup>(a) M. Foltin, G. J. Stueber, and E. R. Bernstein, *J. Chem. Phys.* **111**, 9577 (1999); (b) **114**, 8971 (2001).
- <sup>3</sup>(a) R. Hilbig and R. Wallenstein, *IEEE J. Quantum Electron.* **QE-17**, 1566 (1981); (b) R. H. Page, R. J. Larking, A. H. Kung, Y. R. Shen, and Y. T. Lee, *Rev. Sci. Instrum.* **58**, 1616 (1987); (c) M. P. McCann, C. H. Chen, and M. G. Payne, *J. Chem. Phys.* **89**, 5429 (1988); (d) P. G. Strupp, A. L. Alstrin, R. V. Smilgys, and S. R. Leone, *Appl. Opt.* **32**, 842 (1993); (e) K. Suto, Y. Sato, C. L. Reed, V. Skorokhodov, Y. Matsumi, and M. Kawasaki, *J. Phys. Chem. A* **101**, 1222 (1997); (f) K. Tonokura, T. Murasaki, and M. Koshi, *Chem. Phys. Lett.* **319**, 507 (2000); (g) R. H. Lipson, S. S. Dimov, P. Wang, Y. J. Shi, D. M. Mao, X. K. Hu, and J. Vanstone, *Instrum. Sci. Technol.* **28**, 85 (2000); (h) Y. J. Shi, S. Consta, A. K. Das, B. Maliik, D. Lacey, and R. H. Lipson, *J. Chem. Phys.* **116**, 6990 (2002).
- <sup>4</sup>D. N. Shin, Y. Matsuda, and E. R. Bernstein, *J. Chem. Phys.* **120**, 4150 (2004), previous paper.
- <sup>5</sup>M. Foltin, G. Stueber, and E. R. Bernstein, *J. Chem. Phys.* **109**, 4342 (1998).
- <sup>6</sup>(a) H.-S. Im and E. R. Bernstein, *J. Phys. Chem. A* **106**, 7565 (2002); (b) M. Foltin, G. J. Stueber, and E. R. Bernstein, *J. Chem. Phys.* **109**, 4342 (1998).
- <sup>7</sup>(a) L. Lian, C.-X. Su, and P. B. Armentrout, *J. Chem. Phys.* **97**, 4072 (1992); (b) J. B. Griffin and P. B. Armentrout, *ibid.* **106**, 4448 (1997).